Tetraphenylethylene-BODIPY aggregation-induced emission luminogens for near-infrared polymer light-emitting diodes

Sebnem Baysec[1], Alessandro Minotto[2], Patrick Klein[1], Simone Poddi[2], Andrea Zampetti[2], Sybille Allard[1], Franco Cacialli[2] & Ullrich Scherf[1*]

[1]*Macromolecular Chemistry and Institute for Polymer Technology, Bergische Universität Wuppertal, Wuppertal 42097, Germany;*
[2]*Department of Physics and Astronomy and London Centre for Nanotechnology, University College London, London, WC1E 6BT, UK*

The aggregation-induced emission (AIE) phenomenon provides a new direction for the development of organic light-emitting devices. Here, we present a new class of emitters based on 4,4-difluoro-4-bora-3*a*,4*a*-diaza-*s*-indacene (BODIPY), functionalized at different positions with tetraphenylethylene (TPE), which is one of the most famous AIE luminogens. Thanks to this modification, we were able to tune the photoluminescence of the BODIPY moiety from the green to the near-infrared (NIR) spectral range and achieve PL efficiencies of ~50% in the solid state. Remarkably, we observed an enhancement of the AIE and up to ~100% photoluminescence efficiencies by blending the TPE-substituted BODIPY fluorophores with a poly[(9,9-di-*n*-octylfluorene-2,7-diyl)-*alt*-(benzo[2,1,3]thiadiazol-4,7-diyl)] (F8BT) matrix. By incorporating these blends in organic light-emitting diodes (OLEDs), we obtained electroluminescence peaked in the range 650–700 nm with up to 1.8% external quantum efficiency and ~2 mW/cm^2 radiance, a remarkable result for red/NIR emitting and solution-processed OLEDs.

BODIPY, organic light-emitting diode, aggregation-induced emission, NIR emission, photoluminescence, electro luminescence

1   Introduction

Recent developments in many fields of modern science and medicine show that oligomeric and polymeric dyes absorbing or emitting in the red/near-infrared (NIR) region (650–900 nm) have great importance [1–3]. The NIR dye can be either attached as a side chain or incorporated into the oligomer or polymer backbone. The main advantages of such dyes are a high homogeneity of the resulting active layer, an enhanced processability and high stability [4].

Among several organic fluorescent dyes, BODIPY (4,4′-difluoro-4-bora-3*a*,4*a*-diaza-*s*-indacene) still retains popularity due to its excellent spectroscopic features such as a high absorption coefficient, narrow absorption and emission bands, high fluorescence quantum yields in solution (Φ_F>0.5), and excellent chemical and photostability [5–7]. Furthermore, the emission band can be spectrally tuned from the green to the NIR spectral range by chemical modification of the BODIPY molecular core. However, as most other organic dyes, BODIPY and its derivatives suffer from aggregation quenching and small Stokes shifts which limits their applications in organic electronics, for instance in organic light-emitting diodes (OLEDs).

A promising approach to improve the photophysical properties of BODIPY is to promote aggregation-induced emission (AIE) behavior by incorporating the most prominent member of the AIE organic luminogen family: tetraphenylethylene (TPE). The AIE-active luminogen shall

improve the solid-state emission properties of BODIPY by overcoming the aggregation-caused quenching (ACQ) problem while maintaining the already mentioned advantages of the BODIPY chromophore [8–13]. Design and application of AIE luminogens are a hot research topic since the AIE phenomenon was first reported in 2001 by Tang and co-workers [14]. AIE luminogens are poorly emissive in dilute solutions but form highly emissive aggregates in the condensed state, e.g., either by addition of a non-solvent or in the solid state. The AIE effect is mainly due to the propeller-shape structure of the luminogens, which cause restriction of intramolecular rotations upon aggregation [15].

To our best knowledge, only few articles [16–23] have investigated the substitution of BODIPY with varying numbers of AIE active aryl substituents in different positions, with substitution in 8-position of BODIPY allowing for the most distinct variation of the aggregated state emission.

In this context, our study provides a systematic investigation of substitution effects (alkyl substituents, number of TPE groups) and their consequences on the OLED performance. The materials exhibit Φ_F reaching up to 50% in the solid state as neat thin films and up to 100% when embedded in a blend with poly[(9,9-di-*n*-octylfluorene-2,7-diyl)-*alt*-(benzo[2,1,3]thiadiazol-4,7-diyl)] (F8BT). By sandwiching such blends between conventional electrodes, we obtained OLEDs exhibiting electroluminescence (EL) peaked in the range 650–700 nm, with up to 1.8% external quantum efficiency (EQE) and 2 mW/cm² radiance, which are among the highest values reported so far for fully solution-processed red/NIR emitting OLEDs not leveraging phosphorescence.

2   Experimental

2.1   Synthesis

The starting materials (2-bromo-1,2-diphenylvinyl) benzene and 4-formylphenylboronic acid were obtained from commercial suppliers and used without further purification. The obtained triphenylvinylbenzaldehyde (**1**) was condensed with the corresponding pyrrole in the presence of trifluoroacetic acid (TFA), followed by oxidative dehydrogenation with 2,3-dichloro-5,6-dicyano-1,4-benzoquinone (DDQ) and complexation with boron trifluoride diethyl etherate (BF$_3$:OEt$_2$) to give the corresponding mono-TPE-substituted BODIPYs (TPEBDP1-2-3). To obtain triple-TPE-substituted BODIPYs, mono-substituted-BODIPYs were reacted with NBS and yielded the corresponding 2,6-dibromo derivatives. In microwave assisted Suzuki couplings, the 2,6-dibromo-substituted BODIPY derivatives are coupled with boronic ester-substituted TPE into 2,6,8-tri-TPE-substituted BODIPYs (3TPEBDP1-2-3) (Scheme 1). For detailed information about procedures see the Supporting Information online.

2.2   Optical characterization

AIE characterization. To understand the AIE features of the materials, their luminescent behavior upon aggregation in aqueous media were investigated by photoluminescence (PL) spectroscopy. Photoluminescence was collected from a Horiba Fluoromax-4 spectrofluorimeter and excitation wavelength for each sample indicated in Section 3.1. For the preparation of samples, dry tetrahydrofuran (THF) was selected as good solvent while water was selected as aggregation-inducing non-solvent. Stock solution were prepared. Aliquots of the stock solution were transferred to 10 mL vials and appropriate amounts of THF were added with a micropipette. Then, water was added dropwise to each vial with increasing fraction (between 0–90 vol% water). The final mixture concentrations were fixed to 10^{-6} M. PL measurements of 10 samples for each compound were performed immediately.

Thin film preparation and optical characterization. Thin films were spin-casted onto fused silica substrates from 10 mg/mL toluene solutions. The films were deposited via spin-coating to obtain a thickness of ~100 nm, measured with a Dektak profilometer (USA). Photoluminescence was collected from an Andor Shamrock 163 spectrograph coupled with an Andor Newton EMCCD (UK). The photoluminescence quantum yield (PLQY) experiments were carried out using an integrating sphere setup. For all PL experiments, samples were excited by using 450 and 520 nm laser diodes (average power below 1 mW). Time-resolved PL measurements were carried out with a time-correlated single photon counting (TCSPC) spectrometer as previously reported [24].

2.3   OLEDs fabrication and characterization

OLEDs were fabricated by sandwiching the AIE films between indium-tin oxide (ITO)/PEDOT:PSS anodes and Ca/Al cathodes. ITO substrates were cleaned with acetone and isopropanol in an ultrasonic bath and treated in an O$_2$ plasma chamber for 10 min. A 40 nm layer of PEDOT:PSS (Sigma Aldrich, USA) was spin-coated at 5000 r/min from a 2.8 wt% dispersion in water and annealed at 150 °C for 10 min. The active layer was spin-coated on top of the annealed PEDOT:PSS in N$_2$ environment from the same 10 mg/mL toluene solutions used for the optical characterization in the solid state. A Ca/Al (30/200 nm) cathode was thermally evaporated on top. The samples were then encapsulated with a UV curable epoxy resin (OSSILA E132) and measured in air using a Keithley 2400 source meter (USA) for both the current measurement and the voltage supply. The optical output of the polymer light-emitting diode (PLEDs) was measured with a calibrated silicon photodiode and the EL spectra were collected with the same spectrometer employed
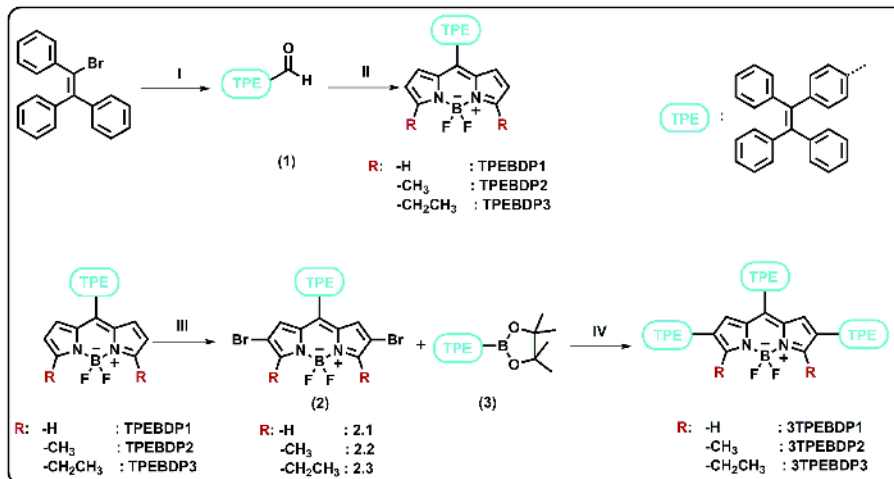
Scheme 1 Synthesis route to TPE substituted BODIPYs (I: (4-formylphenyl) boronic acid, TBAB, Pd(Ph$_3$)$_4$, toluene. II: corresponding pyrrole, TFA, DDQ, Et$_3$N, BF$_3$:OEt$_2$, DCM. III: NBS, DCM:DMF (50:50). IV: K$_2$CO$_3$, Pd(Ph$_3$)$_4$, THF:water (80:20) (color online).

for the PL experiments.

3   Results and discussion

3.1   Aggregation-induced emission characterization

The photoluminescence spectra of TPEBDPx and 3TPEBDPx series were investigated in THF/water mixtures with increasing water fraction (in vol%). By this method, solvent polarity and, corresponding, amount of aggregation were fine-tuned.

The PL spectra of mono-TPE-substituted BODIPYs (TPEBDPx) are shown in Figure 1. TPEBDP2 and TPEBDP3 in THF solutions have an emission around 530 nm (excitation wavelength: 511 nm) due to BODIPY core. With gradual addition of water into THF, the emission is reduced and bathochromically shifted to 609 nm for TPEBDP2 and 640 nm for TPEBDP3. Such a large bathochromic shift of PL can also be visually perceived by the color change of solutions, both under daylight and UV illumination (Figure S1, Supporting Information online). TPEBDP2 has already been reported by Tang *et al.* [16], who investigated also the effect of solvent polarity and temperature on the emission. Namely, they demonstrated that the spectral changes upon increasing solvent polarity can be explained by the AIE effect and the concomitant formation of twisted intramolecular charge-transfer (TICT) states. As shown in Figure S4, TPEBDP3 emission shows a trend similar to the one reported by Tang when measured in solvents with different polarity. Furthermore, for both TPEBDP2 and TPEBDP3, the molecules start to show the AIE effect at 80 vol% water (Figure 1(d)). However, the starting emission intensity is not fully recovered to its highest value at 90 vol% water.

In case of TPEBDP1 (Figure 1(a)), the emission in THF is

peaked at ~670 nm (excitation wavelength: 501 nm). As the water content is increased, the intensity of emission first decreases. Starting from 80 vol% water TPEBDP1 shows an obvious AIE effect with a weak blue-shift of the emission ($\lambda_{\text{max em}}$: 658 nm). It is likely that the lack of alkyl substituents promotes the formation of aggregates at higher water contents. The maximum of fluorescence is achieved for 90 vol% water.

The PL spectra of the three tri-TPE-substituted BODIPYs (3TPEBDPx) are shown in Figure 2. The emission maxima in THF are observed at 689, 646, and 648 nm, respectively. With gradual increase of water content in the THF/water mixture, PL intensities decreased up to 60 vol%, 40 vol%, and 50 vol% water fractions respectively for 3TPEBDP1-2-3. Continued water addition causes aggregate formation which results in increased PL intensities with reaching the highest value at 90 vol% water. The PL intensity of the aggregated samples (90% water) is ca. 1.53 times higher for 3TPEBDP1, if compared to pure THF solution, 1.50 times higher for 3TPEBDP2, and 1.40 times higher for 3TPEBDP3, thus showing a clear, but moderate AIE effect (Figure 2(d)).

The addition of two extra TPE units to the TPEBDPx series induces a more pronounced AIE effect, as expected due to the increased number of rotor units if compared to the mono-TPE-substituted analogues.

3.2   Optical properties in the solid state

The solid-state absorption and photoluminescence properties of the TPEBDPx and 3TPEBDPx series was carried out with thin films deposited from 10 mg/mL toluene solutions by spin coating. Toluene as solvent allows to obtain uniform films. Homogeneity of the emitting layer is indeed an important prerequisite to fabricate efficient light-emitting devices. The absorption and PL spectra of these films are
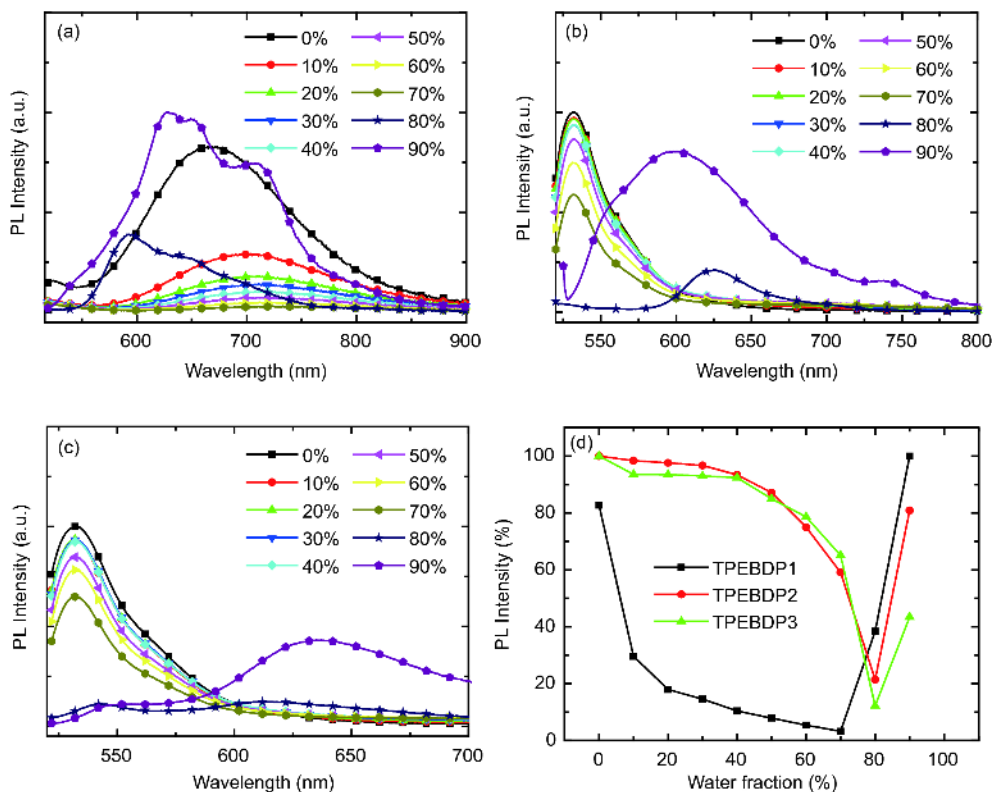
Figure 1 PL spectra of (a) TPEBDP1, (b) TPEBDP2, (c) TPEBDP3 in THF/water mixtures at different water contents. (d) The change of PL intensity with increasing water fraction (color online).
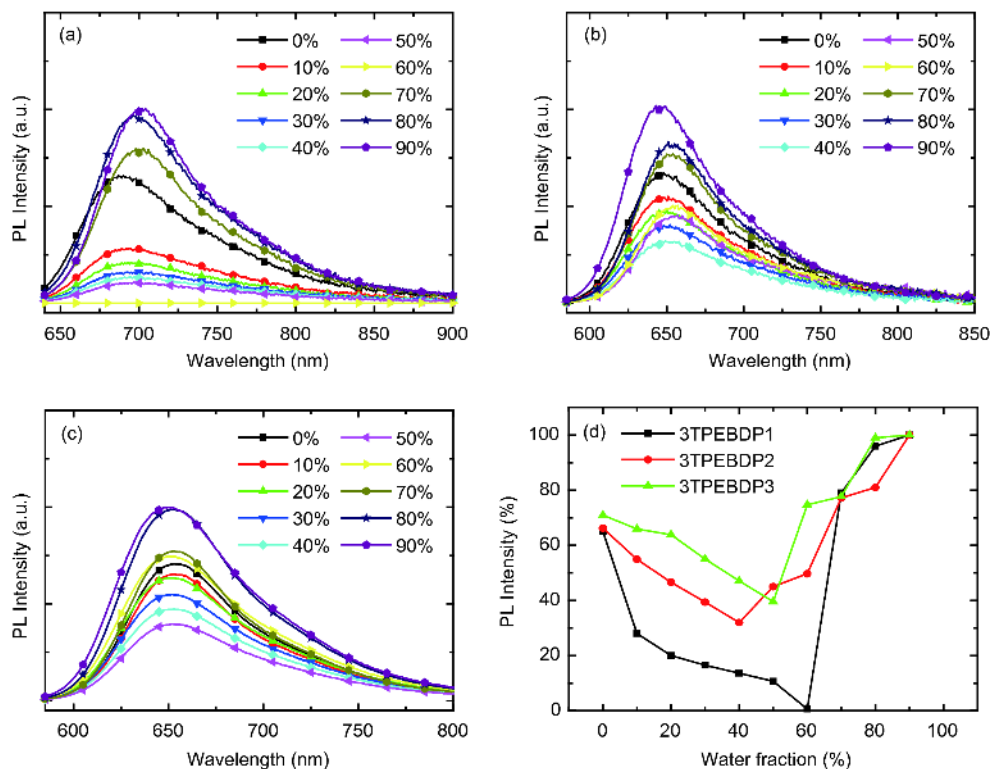
Figure 2 PL spectra of (a) 3TPEBDP1, (b) 3TPEBDP2, (c) 3TPEBDP3 in THF/water mixtures of different water contents. (d) The change of PL intensity with increasing water fraction (color online).

presented in Figure 3.

The absorption spectra of the mono-TPE substituted molecules (TPEBDPx) are dominated by the absorption component of the BODIPY moiety peaking at ~520 nm. Most likely due to aggregation, we also observe a broadening and a 10 nm red-shift of these bands when moving from solution to film. Whereas in solution TPEBDP2 and TPEBDP3 exhibit a PL emission peaked at 525 nm with full width at half maximum (FWHM) of only 30 nm, which is typical of 2,6-unsubstituted BODIPYs [25], the PL spectra from the corresponding spin-casted films exhibit broad PL spectra with maxima at 615 nm for TPEBDP2 and 650 nm for TPEBDP3. Such a substantial (>100 nm) Stokes shift is most likely the result of aggregation in the solid-state, in analogy to what is observed in water:THF solutions with large water (non-solvent) percentages (Figure 1). Regarding the α-unsubstituted TPEBDP1, we note that both solution and film present a PL peaking at 670 nm.

Looking at the tri-TPE substituted molecules (3TPEBDPx), we observe a substantial red-shift of the absorption and emission spectra compared to the TPEBDPx series, reaching up to 120 nm for 3TPEBDP1. Furthermore, in contrast to what is observed with TPEBDP1-2-3, both absorption and emission spectra of the 3TPEBDP1-2-3 molecules in the solid state (Figure 3) are only slightly red-shifted (10–20 nm) and broader compared to those measured in solution. Namely, the absorption spectra are dominated by a broad band in the 500–650 nm spectral region and maxima at 580 nm for 3TPEBDP2 and 3, and in the 550–700 nm range with maximum at 635 nm for 3TPEBDP1. Concerning the PL, spectra measured from 3TPEBDP2 and 3 films peak at 670 nm, whereas the PL of 3TPEBDP3 shows a maximum in the NIR at 720 nm.

To verify the presence of AIE effect, we measured also the PL quantum efficiency Φ_F of each film and collected the corresponding values in Table 1.

With the exception of 3TPEBDP1, all oligomers show similar or slightly higher Φ_F for the solid-state films if compared to the solution values. Notably, 3TPEBDP2 and 3 in the solid-state show Φ_F of 39% and 48%, respectively, which are relatively high and not easily attainable with
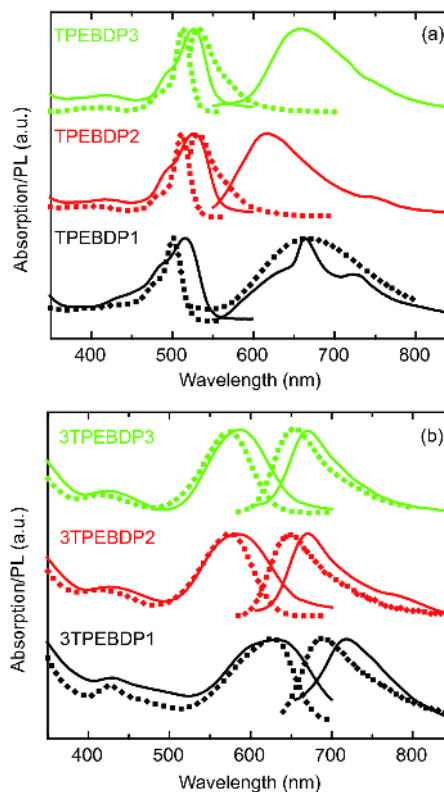
Figure 3 Absorption and emission of TPEBDPx (a) and 3TPEBDPx (b) in diluted THF solution (dotted lines) and solid-state thin films (full lines). For the PL experiments, samples were excited with a 520 nm laser diode (average power <1 mW) (color online).

conventional molecular chromophores when spin-coated from solution as neat films. For completeness, we report in Figure S10 and Table S2 (Supporting Information online) also the PL spectra and corresponding Φ_F obtained from films deposited from THF solutions. By comparing the spectra from the films obtained from toluene (Figure 3) and those obtained from THF (Figure S10), no major variations can be detected. Furthermore, for TPEBDPx molecules, the Φ_F values reported in Table S2 for the films spin-coated from THF are similar to those obtained from toluene (Table 1). On the contrary, due to additional TPE units for the 3TPEBDPx dyes, we note a remarkable variation, especially for the most

Table 1 PL quantum efficiency (Φ_F), highest occupied molecular orbital (HOMO) and lowest occupied molecular orbital level (LUMO) energy levels. PL efficiency values are to be considered with a 10% uncertainty on the absolute value. For the PL efficiency experiments, samples were excited with a 520 nm laser diode (average power below 1 mW). HOMO values were determined by atmospheric pressure photo-electron spectroscopy (AC-2), LUMO=Eg(opt) −HOMO(AC-2), See Eg(opt) values in Table S2

Compound	Φ_F sol (%)	Φ_F film (%)	HOMO (eV)	LUMO (eV)
TPEBDP1	8	10	−5.63	−3.39
TPEBDP2	4	4	−5.84	−3.64
TPEBDP3	4	5	−5.82	−3.59
3TPEBDP1	47	10	−5.69	−3.96
3TPEBDP2	29	39	−5.69	−3.82
3TPEBDP3	44	48	−5.65	−3.78

efficient 3TPEBDP2 and 3 dyes. Namely, for the films obtained from THF solutions we obtained Φ_F values reaching up to 68% for 3TPEBDP2 and 98% for 3TPEBDP3. However, such films were highly inhomogeneous and, by exciting different areas of the sample and different samples, we measured efficiencies below 40% for both molecules.

3.3   Aggregation-induced emission in F8BT blends

Given that we obtained the highest PL efficiencies from the 3TPEBDPx series, with 3TPEBDP2 and 3 benefitting from the AIE effect in the solid-state, we decided to focus on these materials to fabricate OLEDs. Furthermore, 3TPEBDPx molecules, here presented for the first time, are attractive also because a good fraction of their emission (78%, 43% and 35% for 3TPEBDP1, 2 and 3, respectively) is in the NIR (>700 nm). In this spectral range, PL efficiencies up to 50% in the solid state (Table 1) are, in general, difficult to achieve, mainly due to ACQ and the so-called "Energy-gap law" [26].

To maximize the performance of the final devices, we incorporated the 3TPEBDPx molecules in a solid-state blend with F8BT, as well-established green emitting semiconducting polymer [2]. Among the plethora of commercially available semiconducting polymers, we selected F8BT as polymer host for mainly two reasons: first of all, its emission perfectly overlaps with the absorption of 3TPEBDPx, thereby affording efficient energy transfer to the red/NIR emitting moieties. Secondly, and most importantly, the HOMO (−6.0 eV) and LUMO (−3.3 eV) of F8BT enable the formation of a "so-called" type I or straddling heterojunction when blended with 3TPEBDPx molecules, whose energies of the frontier molecular orbitals are collected in Table 1. Namely, the 3TPEBDPx narrower energy bandgap is completely encompassed by the F8BT larger one, so as to form a straddling heterojunction, which favors exciton localization and prevents exciton dissociation.

Prior to integration of the blends into OLEDs, we characterized the optical properties of such solid-state mixtures, also to identify if the AIE effect is conserved. To this aim, we investigated different concentrations of 3TPEBDPx molecules in F8BT, to find out that the best results in terms of

quenching of the residual F8BT emission and PL efficiency are obtained, for all 3TPEBDPx moieties, from 3TPEBDPx: F8BT blends with 1 *w/w*% of 3TPEBDPx loading. The absorption and corresponding emission spectra of such films are illustrated in Figure 4, whereas Φ_F values are collected in Table 2.

By looking at the absorption spectra in Figure 4, we note that the extinction profile is dominated by the F8BT absorption. Nonetheless, at only 1 *w/w*% of 3TPEBDPx concentration, the emission from the F8BT host is almost completely quenched for all three combinations, thanks to the efficient resonant energy transfer from the polymeric host to the emitters. Among the three molecules, 3TPEBDP1 is the one in which the ratio between the F8BT and acceptor PL is higher.

However, not only is 3TPEBDP1:F8BT the blend exhibiting the most prominent green emission from the host, but also, looking at Table 2, 3TPEBDP1:F8BT films are those exhibiting the lowest Φ_F. This means that, although Φ_F values increase from 10% to 47% when embedded in F8BT (Table 2), aggregation quenching affects the 3TPEBDP1 PL performance also when in blend with F8BT and prevents the attainment of higher PL efficiencies. On the other hand, 3TPEBDP2 and 3TPEBDP3 1 *w/w*% blends display Φ_F~100%, and almost no residual green emission from
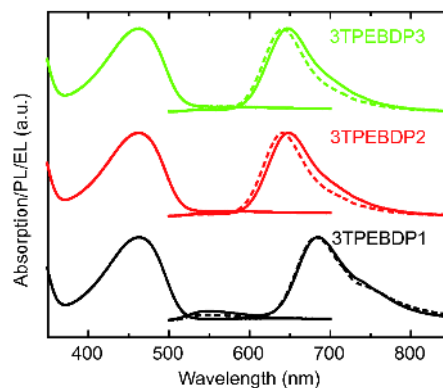
Figure 4   Absorption, PL and EL spectra (dashed lines) of 3TPEBDPx: F8BT blends with 1 *w/w*% of 3TPEBDPx loading. The absorption spectra of the blends are dominated by the F8BT band peaking at 460 nm (color online).

Table 2   PL quantum efficiency (Φ_F) of neat films and 0.1 and 1 *w/w*% 3TPEBDP1:F8BT blends, PL lifetime and calculated radiative (k_R) and non-radiative (k_{NR}) rate. PL efficiency values are to be considered with a 10% uncertainty on the absolute value. For the PL efficiency experiments on the blends, samples were excited with a 450 nm laser diode (average power below 1 mW) to selectively excite the F8BT matrix

film	Φ_F film (%)	τ (ns)	k_R (ns^{-1})	k_{NR} (ns^{-1})
neat 3TPEBDP1	10	0.68	0.15	1.33
1% 3TPEBDP1	47	2.7	0.17	0.20
neat 3TPEBDP2	39	1.01	0.39	0.60
1% 3TPEBDP2	96	4.29	0.22	0.01
neat 3TPEBDP3	48	1.34	0.36	0.38
1% 3TPEBDP3	100	4.56	0.22	0

F8BT. We tested also higher doping levels for 3TPEBDP2 and 3TPEBDP3 (up to 50 *w/w*%), but we observed a decrease of the efficiency when the 3TPEBDPx content exceeded 1%. Therefore, we conclude that the 1% 3TPEBDP2 and 3TPEBDP3 concentration is optimal for maximizing both the PLQY and energy transfer from F8BT.

We have also measured the PL decay lifetimes of both the bare 3TPEBDPx films and blends. The evolution of the PL decay at varying 3TPEBDPx concentration is illustrated in Figure S6, whereas the decay lifetimes (τ) and the radiative (k_R) and non-radiative (k_{NR}) decay rates are reported in Table 2. We obtained k_R and k_{NR} via the relations $\Phi_F = k_R/(k_R + k_{NR})$ and $\tau = 1/(k_R + k_{NR})$. Importantly, we note that the k_R and k_{NR} values reported in Table 2 for the blends are probably less accurate compared to those of the neat films, as part of the emitted photons that account for the corresponding Φ_F originate from the unquenched F8BT matrix (Figure 4). However, such an approximation in the calculation of k_R and k_{NR} is reasonably plausible, given the substantial increase of τ and Φ_F when 3TPEBDPx molecules are embedded in F8BT.

Looking first at the neat 3TPEBDPx films, Table 2 shows that k_R for 3TPEBDP1 is about half compared to the one of 3TPEBDP2 and 3TPEBDP3. Such a lower radiative rate further supports the discussion above, confirming that intermolecular interactions, and therefore ACQ, are more effective in 3TPEBDP1 films compared to the others. Furthermore, 3TPEBDP1 films also show non-radiative rates that are more than twice as high compared to the other compounds. This suggests a limited AIE-induced enhancement of 3TPEBDP1 PL efficiency, at least in the solid state.

Moving to the blends, as suggested already from the increasing Φ_F, the AIE-effect is verified for all systems, i.e., k_{NR} is reduced to a much larger extent compared to k_R. For 3TPEBDP2 and 3TPEBDP3, this conclusion is somehow trivial, given that the Φ_F in F8BT is $\sim 100\%$, undoubtedly meaning that all non-radiative exciton recombination processes, including intermolecular rotations, are precluded more efficiently than in the neat films. However, it is worth highlighting that, although $k_{NR} \sim 0$, also k_R decreases by a factor of about two, suggesting that intermolecular interactions, either in the ground state or in the excited state (excimer or exciplex formation), are probably enhanced in the blends compared to the neat film.

Concerning F8BT:3TPEBDP1 blends, k_{NR} is reduced even more dramatically from 1.3 ns^{-1} down to 0.2 ns^{-1}, meaning

that the effectiveness of the non-radiative processes responsible for the quenching of the Φ_F of 3TPEBDP1 from 47% in solution to 10% in film (Table 1) is mitigated when 3TPEBDP1 is diluted in a F8BT matrix. On the other hand, k_R exhibits only a slight increase from 0.15 to 0.17 ns^{-1} in the 1% blend, although the residual F8BT emission might also account for such a little variation compared to the factor of two decrease of k_R observed for 3TPEBDP2 and 3TPEBDP3. This results also mean that, in analogy to what is observed for 3TPEBDP2 and 3TPEBDP3, dilution in F8BT does not suppress intermolecular interactions between 3TPEBDP1 molecules. Besides, electronic interactions between 3TPEBDPx and F8BT chains cannot be ruled out either.

3.4 OLEDs

Finally, given the extremely high PL efficiencies we obtained from the F8BT:3TPEBDPx blends, we used them to fabricate OLEDs, with the architecture and deposition techniques described in the experimental section. The electroluminescence (EL) spectra of such blends are reported in Figure 4, whereas the density-voltage-radiance (JVR) and external quantum efficiency (EQE) versus current density curves are reported in Figure 5. OLEDs characteristics are summarised in Table 3.

By looking at Figure 4, we observe that EL spectra of the blends show only a slight (~5 nm) blue-shift compared to the PL ones. Furthermore, as for the PL, the EL from the F8BT host is efficiently quenched in favor of the red/NIR emission from the 3TPEBDPx dopant. In terms of device performance, we obtained the best efficiencies from the F8BT:3TPEBDP2 blend, which exhibited an average EQE of 1.47%, with a peak value at 1.82%. Such values are remarkably high, considering that we achieved them from solution-processed devices, not optimized for charge injection/transport and photon out-coupling. Moreover, the maximum radiance reaches up to 2 mW/cm^2 with F8BT:3TPEBDP2 devices, with a turn-on voltage as low as 3 V.

Although slightly less efficient (maximum EQEs up to 1.3%), also devices incorporating the F8BT:3TPEBDP3 blend exhibited radiances up to 2 mW/cm^2, and $V_{ON} \sim 3$ V. Notably, whereas the EL V_{ON} of both F8BT:3TPEBDP2 and F8BT:3TPEBDP3 blends match the one of the neat F8BT devices (Figure S11), the EQE and radiance values reported

Table 3 OLEDs summary of the device characteristics of F8BT:3TPEBDPx OLEDs

Sample	V_{ON} (V)	Radiance (mW/cm^2)	EQE$_{MAX}$ (%)[a]	EQE$_{MAX}$ (%)[b]
1% 3TPEBDP1	4.3±0.6	0.91±0.55	0.51±0.37	1.29
1% 3TPEBDP2	3.2±0.3	1.60±0.18	1.47±0.21	1.82
1% 3TPEBDP3	3±0.2	1.62±0.41	1.16±0.13	1.31

a) Average maximum EQE. b) Maximum EQE.
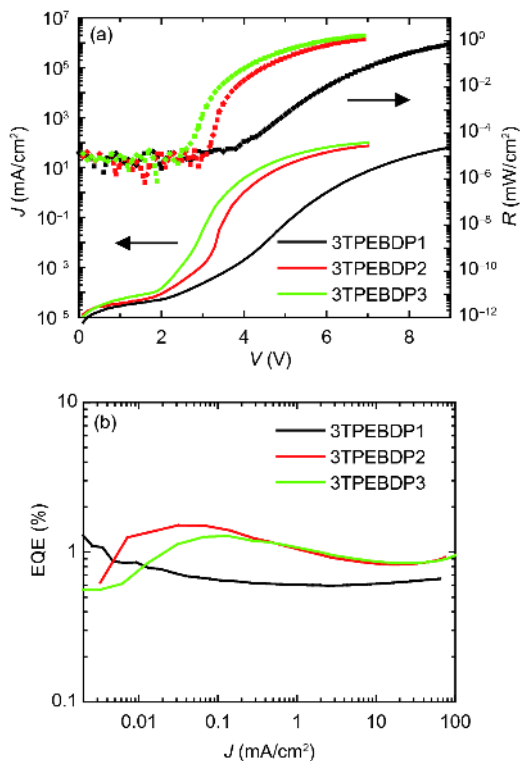
Figure 5 (a) JVR curves and (b) EQE versus current density plot of OLEDs incorporating F8BT: 3TPEBDPx 1% blends (color online).

in Table 3 exceed those we measured from the undoped F8BT OLEDs, for which the maximum EQE and radiance we measured are 0.86% and 1.1 mW/cm^2, respectively.

4   Conclusions

In summary, we have synthesized red/NIR emitting mono-TPE-substituted and tri-TPE-substituted BODIPY derivatives and investigated their AIE properties. Due to the high solid-state emission of tri-TPE-substituted materials, OLED devices performed and attained EQE values exceeding 1% from NIR emitting 3TPEBDP1-2-3/F8BT blends as "metal-free" active layer. To the best of our knowledge, such efficiencies, together with low turn-on voltage (2.5–4 V) and radiances reaching up to 2 mW/cm^2, are unprecedented for AIE OLEDs emitting in this spectral range (600–800 nm) and fabricated via solution processing. Further optimization can lead to progresses of these emitters for the use of biomedical and communication purposes.

Supporting information   The supporting information is available online at http://chem.scichina.com and http://link.springer.com/journal/11426. The supporting materials are published as submitted, without typesetting or editing. The responsibility for scientific accuracy and content remains entirely with the authors.

1   Boens N, Leen V, Dehaen W. *Chem Soc Rev*, 2012, 41: 1130–1172
2   Zampetti A, Minotto A, Squeo BM, Gregoriou VG, Allard S, Scherf U, Chochos CL, Cacialli F. *Sci Rep*, 2017, 7: 1611
3   Murto P, Minotto A, Zampetti A, Xu X, Andersson MR, Cacialli F, Wang E. *Adv Opt Mater*, 2016, 4: 2068–2076
4   Marechal E. *Prog Org Coatings*, 1982, 10: 251–287
5   Ulrich G, Ziessel R, Harriman A. *Angew Chem Int Ed*, 2008, 47: 1184–1201
6   Loudet A, Burgess K. *Chem Rev*, 2007, 107: 4891–4932
7   Ziessel R, Ulrich G, Harriman A. *New J Chem*, 2007, 31: 496
8   Chen M, Li L, Nie H, Tong J, Yan L, Xu B, Sun JZ, Tian W, Zhao Z, Qin A, Tang BZ. *Chem Sci*, 2015, 6: 1932–1937
9   Dong W, Pina J, Pan Y, Preis E, Seixas de Melo JS, Scherf U. *Polymer*, 2015, 76: 173–181
10   Zhao Z, Chen S, Lam JWY, Wang Z, Lu P, Mahtab F, Sung HHY, Williams ID, Ma Y, Kwok HS, Tang BZ. *J Mater Chem*, 2011, 21: 7210
11   Zhao Z, Chen S, Lam JWY, Lu P, Zhong Y, Wong KS, Kwok HS, Tang BZ. *Chem Commun*, 2010, 46: 2221
12   Zhao Q, Zhang S, Liu Y, Mei J, Chen S, Lu P, Qin A, Ma Y, Sun JZ, Tang BZ. *J Mater Chem*, 2012, 22: 7387
13   Yuan WZ, Lu P, Chen S, Lam JWY, Wang Z, Liu Y, Kwok HS, Ma Y, Tang BZ. *Adv Mater*, 2010, 22: 2159–2163
14   Luo J, Xie Z, Lam JWY, Cheng L, Tang BZ, Chen H, Qiu C, Kwok HS, Zhan X, Liu Y, Zhu D. *Chem Commun*, 2001, 18: 1740–1741
15   Mei J, Hong Y, Lam JWY, Qin A, Tang Y, Tang BZ. *Adv Mater*, 2014, 26: 5429–5479
16   Gomez-Duran CFA, Hu R, Feng G, Li T, Bu F, Arseneault M, Liu B, Peña-Cabrera E, Tang BZ. *ACS Appl Mater Interfaces*, 2015, 7: 15168–15176
17   Hu R, Lager E, Aguilar-Aguilar A, Liu J, Lam JWY, Sung HHY, Williams ID, Zhong Y, Wong KS, Peña-Cabrera E, Tang BZ. *J Phys Chem C*, 2009, 113: 15845–15853
18   Baglan M, Ozturk S, Gür B, Meral K, Bozkaya U, Bozdemir OA, Atılgan S. *RSC Adv*, 2013, 3: 15866
19   Li Q, Qian Y. *New J Chem*, 2016, 40: 7095–7101
20   Li Z, Chen Y, Lv X, Fu WF. *New J Chem*, 2013, 37: 3755
21   Hu R, Gómez-Durán CFA, Lam JWY, Belmonte-Vázquez JL, Deng C, Chen S, Ye R, Peña-Cabrera E, Zhong Y, Wong KS, Tang BZ. *Chem Commun*, 2012, 48: 10099
22   Zhao Z, Chen B, Geng J, Chang Z, Aparicio-Ixta L, Nie H, Goh CC, Ng LG, Qin A, Ramos-Ortiz G, Liu B, Tang BZ. *Part Part Syst Charact*, 2014, 31: 481–491
23   Gao H, Gao Y, Wang C, Hu D, Xie Z, Liu L, Yang B, Ma Y. *ACS Appl Mater Interfaces*, 2018, 10: 14956–14965
24   Petrozza A, Brovelli S, Michels JJ, Anderson HL, Friend RH, Silva C, Cacialli F. *Adv Mater*, 2008, 20: 3218–3223
25   Tram K, Yan H, Jenkins HA, Vassiliev S, Bruce D. *Dyes Pigments*, 2009, 82: 392–395
26   Englman R, Jortner J. *Mol Phys*, 1970, 18: 145–164